ISSN 1674-1056
http://cpb.iphy.ac.cn
http://iopscience.iop.org/cpb
中国物理 B
Chinese Physics
中国物理 Chinese Physics B

# Shared aperture metasurface antenna for electromagnetic vortices generation with different topological charges

He Wang(王贺), Yong-Feng Li(李勇峰), and Shao-Bo Qu(屈绍波)
**Citation:**Chin. Phys. B, 2021, 30 (**8**): 084101. DOI: 10.1088/1674-1056/abe37c
Journal homepage: http://cpb.iphy.ac.cn; http://iopscience.iop.org/cpb

**What follows is a list of articles you may be interested in**

---

## A novel receiver-transmitter metasurface for a high-aperture-efficiency Fabry-Perot resonator antenna

Peng Xie(谢鹏), Guangming Wang(王光明), Binfeng Zong(宗彬锋), and Xiaojun Zou(邹晓鋆)
Chin. Phys. B, 2021, 30 (**8**): 084103. DOI: 10.1088/1674-1056/ac0788

## Characteristic mode analysis of wideband high-gain and low-profile metasurface antenna

Kun Gao(高坤), Xiang-Yu Cao(曹祥玉), Jun Gao(高军), Huan-Huan Yang(杨欢欢), and Jiang-Feng Han(韩江枫)
Chin. Phys. B, 2021, 30 (**6**): 064101. DOI: 10.1088/1674-1056/abdb23

## Ultra-wideband low radar cross-section metasurface and its application on waveguide slot antenna array

Li-Li Cong(丛丽丽), Xiang-Yu Cao(曹祥玉), Tao Song(宋涛), Jun Gao(高军)
Chin. Phys. B, 2018, 27 (**11**): 114101. DOI: 10.1088/1674-1056/27/11/114101

## Design of multi-band metasurface antenna array with low RCS performance

Si-Ming Wang(王思铭), Jun Gao(高军), Xiang-Yu Cao(曹祥玉), Yue-Jun Zheng(郑月军), Tong Li(李桐), Jun-Xiang Lan(兰俊祥), Liao-Ri Ji-Di(吉地辽日)
Chin. Phys. B, 2018, 27 (**10**): 104102. DOI: 10.1088/1674-1056/27/10/104102

## Ultra-thin circularly polarized lens antenna based on single-layered transparent metasurface

Kaiyue Liu(刘凯越), Guangming Wang(王光明), Tong Cai(蔡通), Wenlong Guo(郭文龙), Yaqiang Zhuang(庄亚强), Gang Liu(刘刚)
Chin. Phys. B, 2018, 27 (**8**): 084101. DOI: 10.1088/1674-1056/27/8/084101

---

# Shared aperture metasurface antenna for electromagnetic vortices generation with different topological charges*

He Wang(王贺)†, Yong-Feng Li(李勇峰), and Shao-Bo Qu(屈绍波)

*Department of Basic Sciences, Air Force Engineering University, Xi'an* 710051, *China*

(Received 7 January 2021; revised manuscript received 18 January 2021; accepted manuscript online 5 February 2021)

Vortex beams carrying orbital angular momentum (OAM) have aroused great interest of both scientific and engineering communities. Encouragingly, generating OAM with different topological charges in a shared aperture is regarded as a potential route to expanding the communication capacity, which yet is an academic challenging task. In this work, a paradigm of designing metasurface-based shared aperture antenna for generating polarization-dependent vortex beams with distinct topological charges is proposed. Anisotropic unit cells that can tailor different resonance phase profiles in two orthogonal orientations are used to assemble a metasurface reflector. As a proof-of-concept, a planar reflector antenna is designed with two Vivaldi sources, which can generate *x*- and *y*-polarized vortex beams with topological charges of $l = -1$ and $l = -2$, respectively. Both the simulation results and the measurement results are in good agreement, which demonstrates the feasibility of our design. Significantly, this work provides a new route to achieving vortex beams carrying different topological charges in the same frequency band, which may have potential applications in communication systems.

**Keywords:** metasurface, electromagnetic vortex, antenna, orbital angular momentum

**PACS:** 41.20.–q, 41.20.Jb **DOI:** 10.1088/1674-1056/abe37c

## 1. Introduction

Nowadays, the spectral efficiency and communication capacity have already pressed on Shannon limit.[1] Hence, there is an urgent need to put forward an effective way to solve the difficulty brought by the huge communication data. In the past few years, orbital angular momentum (OAM) with multiple topological charges has been regarded as a potential technology that attracts great attention due to its anti-jam capacity.[2–4]

To date, various methods have been demonstrated to generate OAM, including spiral phase plates,[5–7] spiral reflectors,[8] antenna arrays,[9,10] *etc*. With the development of artificial materials, metasurface has become an alternative tool to design OAM generator due to the advantages of negligible thickness and huge manipulation flexibility.[1,2,5,11–22] Unfortunately, the mechanism of generating OAM by the aforementioned strategies introduces a twist phase profile. Therefore, it is hard to achieve vortex beams with versatile topological charges in a shared aperture. To solve this problem, the method of separating the metasurface aperture into multiple sectors is explored in both light and microwave regions.[16,17] Nevertheless, this method suffers the drawback of inefficiency for each mode. Besides, the generated vortex beams can hardly be received. On the other hand, the strategy of superimposing multi-modes by integrating phase distributions has been studied.[5] However, the superimposed metasurface inevitably introduces additional phase noise, which deteriorates the overall performance of each OAM mode.[18] Although these efforts successfully integrated OAM with multiple modes in a metasurface aperture, it is hard to apply to antennas and wireless propagation systems. To effectively utilize the aperture to generate OAM with different modes, using anisotropic metasurface is a good alternative that can independently manipulate the resonance phases in two orthogonal polarizations.[23,24]

In this work, we propose a strategy to design the shared aperture reflector antenna to achieve the polarization-dependent vortex beams carrying OAM with different topological charges. Using the cross-shaped anisotropic unit cells, the phase distribution can be flexibly manipulated into two orthogonal polarization states. Sharply different from traditional reflect-array configuration that can be used only to generate OAM with a single mode, the proposed strategy provides an alternative way to achieve electromagnetic vortices carrying arbitrary two modes. As a proof-of-concept, vortex beams carrying topological charges of $l = -1$ and $l = -2$ are designed for *x*- and *y*-polarizations, respectively. Two Vivaldi antennas operate as the linearly polarized spot sources, which are obliquely placed at two offset focal points of metasurface reflector. The simulation results and the measurement results support that the proposed shared aperture antenna can work at frequencies of 14 GHz–16 GHz. Owing to the distinct modes of the produced vortex beams, the proposed antenna can be used as dual-polarized reflector antenna that carries different topological charges, which can beapplied to communication

*Project supported by the National Natural Science foundation of China (Grant No. 61971347).

†Corresponding author. E-mail: 18066540235@163.com

© 2021 Chinese Physical Society and IOP Publishing Ltd 

systems.

## 2. Design principle

The conceptual illustration is depicted in Fig. 1, feed antennas I and II are used to produce $x$- and $y$-polarized waves to enable the reflector antenna to generate the OAM with different topological charges.

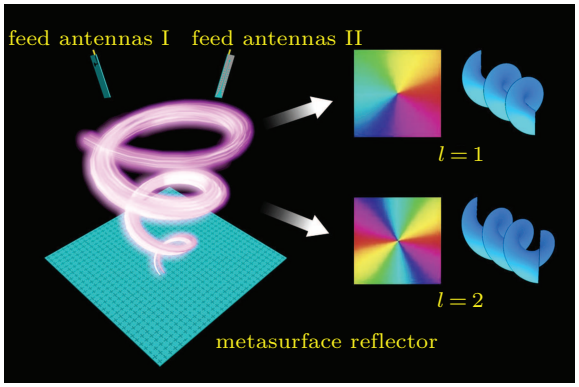



**Fig. 1.** Conceptual illustration of proposed shared aperture antenna.

To achieve independent phase responses in $x$- and $y$-polarization directions, we propose a cross-shaped anisotropic unit cell to assemble the reflector antenna. Topological structure of the proposed unit cell is presented in Fig. 2(a), a cross-shaped metallic pattern is etched on a copper-backed F4B ($\varepsilon_r = 2.65$, $\tan\delta = 0.001$) substrate. The periodical length $p$ is 6.8 mm, and the thickness $d$ is 1.6 mm. The optimized parameters are as follows: $a = 0.6$ mm, $b = 0.2$ mm, and $c = 0.2$ mm. The two arms of cross-shaped unit cell are set to be $l_x$ and $l_y$, respectively. To explain the characteristics of proposed unit cell in detail, we carry out the simulations by Computer Simulation Technology (CST) Microwave Studio. The boundary conditions along $x$ and $y$ axes are set to be "unit cell", and two Floquet ports are applied to $+z$ and $-z$ directions.

To control the incidence of $x$- and $y$-polarized waves independently, the key is to reduce the interference between two arms. Here, to figure out the resonance mechanism of the two arms, the surface current is monitored. The surface current distribution of the unit cell under the $y$-polarized wave at central frequency 15 GHz is given in Fig. 2(b). It is observed that the current intensity is enhanced on the arm along the $y$ axis, while weaken on the arm along the $x$ axis. This phenomenon indicates that the arm along the $y$ direction resonates when illuminated by the $y$-polarized incident wave, while the arm in the $x$ direction is almost non-resonant. Figure 2(c) presents the co-polarization reflection phase $\varphi_{xx}$ and $\varphi_{yy}$ under $x$- and $y$-polarized incidences at 15 GHz. A phase shift from $-112°$ to $-458°$ is acquired for the $y$-polarized wave when $l_y$ varies from 2.5 mm to 6.5 mm under the $y$-polarized incidence. The phase response of the $x$-polarized wave is nearly stable under the same circumstance. In addition, the phase range covers 346° instead of 360°. Therefore, we select the unit cells with phase ranging from 346° to 353° (fixed at 346°) and 353° to 360° (fixed at 0°) in the metasurface design. Here, it should be noted that the similar results can be obtained when $l_x$ varies from 2.5 mm to 6.5 mm due to the structural interchangeability between $l_x$ and $l_y$.

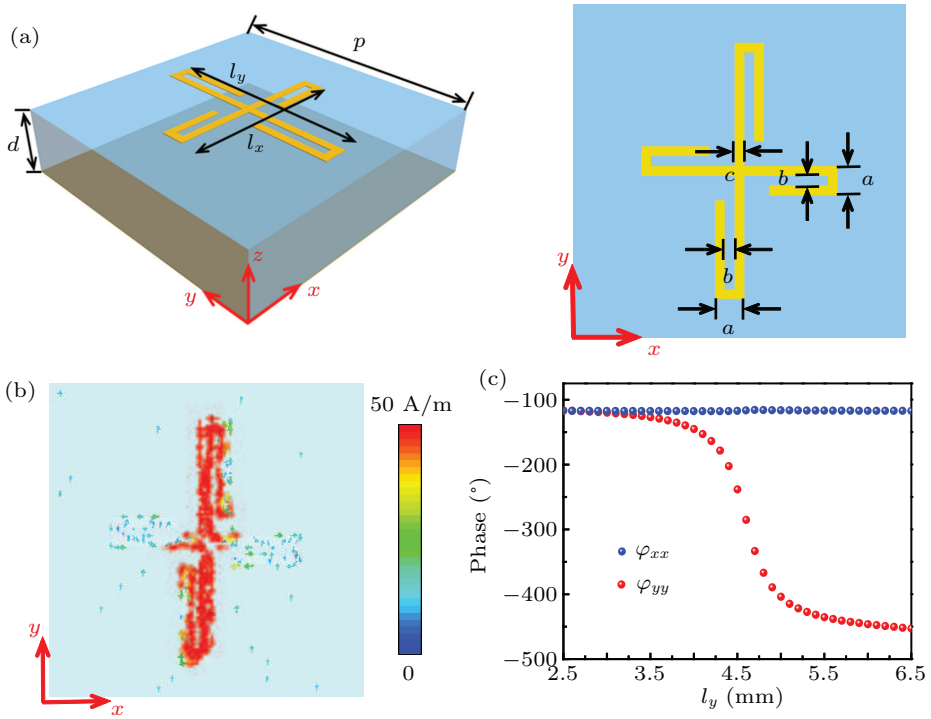



**Fig. 2.** (a) Topological structure of cross-shaped anisotropic unit cell, (b) surface current distribution under $y$-polarized wave at 15 GHz, (c) co-polarization reflection phase under $x$- and $y$-polarized incidences ($\varphi_{xx}$ and $\varphi_{yy}$), with $l_y$ varying from 2.5 mm to 6.5 mm at 15 GHz.

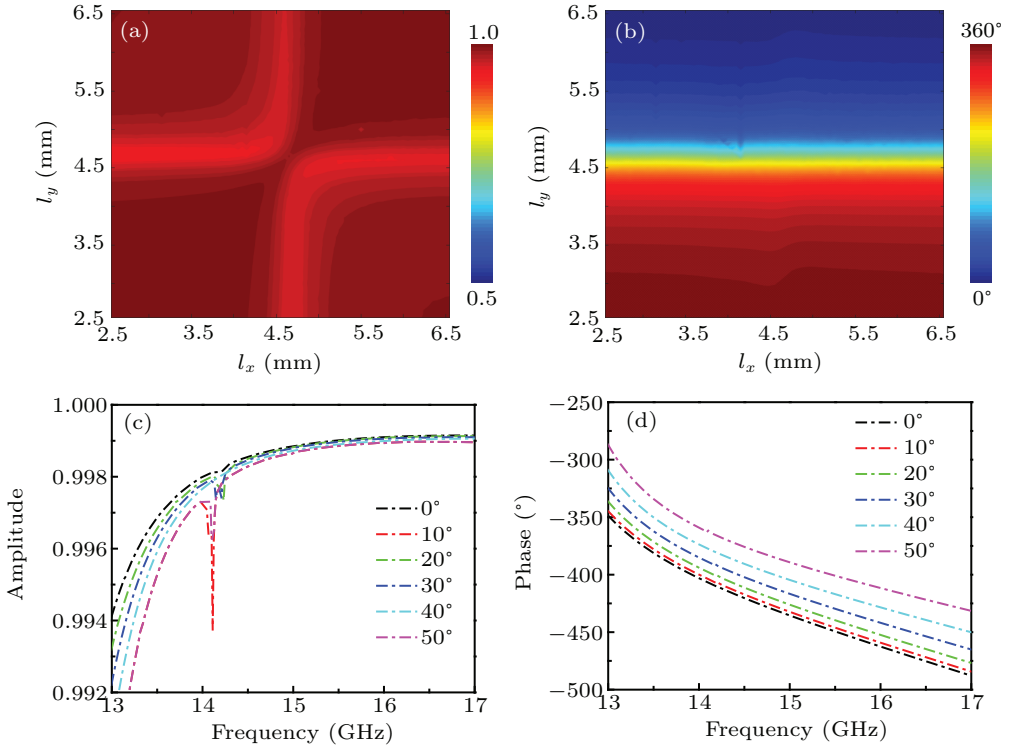



**Fig. 3.** Reflection characteristics of proposed unit cell, showing (a) spectrum of amplitude, (b) spectra of phase, (c) amplitudes under oblique incidence, and (d) phases under oblique incidence.

To intuitively observe the influence of $l_x$ and $l_y$ on the reflection characteristics, figures 3(a) and 3(b) show the spectra of amplitude and phase of $y$ polarization with $l_x$ and $l_y$ both varying from 2.5 mm to 6.5 mm at 15 GHz. Obviously, the reflection amplitude is nearly 1, and the phase change can cover nearly 360° which only follows the variation of $l_y$. These results further manifest the independence between $x$ and $y$ polarizations. Similarly, the same results can be acquired under the incidence of $x$-polarized wave. Hence, the unit cell has the capacity of polarization isolation.

To achieve a vortex beam, the key lies in introducing a transverse cross section of phase coefficient $e^{-il\varphi}$. Suppose that the phase difference between two selected points is $\Delta\varphi$, and the azimuthal angles of these two points are $\theta_1$ and $\theta_2$. Accordingly, the topological charge of $l = \Delta\varphi/(\theta_1 - \theta_2)$ can be acquired. To obtain the vortex beam by a reflective metasurface, it is important to distort the wave-front of reflection wave. Therefore, the spiral phase distribution is adopted. In order to eliminate the phase delay of the spherical wave from the spot sources and produce vortex beams with different topological charges, the phase distribution of the metasurface reflector must satisfy the equation as follows:

$$\varphi(x,y) = \varphi_0 \frac{2\pi}{\lambda}(\sqrt{x^2+y^2+F^2} - F) + l\tan^{-1}(y/x), \quad (1)$$

where $\varphi_0$ is the reflected phase of the unit cell located at the origin position, $\lambda$ is the operating wavelength in free space, and $F$ is focal length. Besides, $l$ is topological number, $\tan^{-1}(y/x)$ is azimuthal angle, which is related to spiral phase distribution. Accordingly, the spherical wave-front can be reshaped into a plane wave-front with spatial distorted phase profile. In order to be match with the boundary conditions of the proposed unit cells, the metasurface aperture is divided into sixteen sectors to introduce the required spiral phase distribution.

Owing to the metasurface reflector being fed by spot sources, the characteristics of unit cell should be stable under oblique incidence. Figures 3(c) and 3(d) depict the simulated amplitude and phase in a frequency range of 13 GHz–17 GHz under different oblique incident angles. It can be clearly observed that the amplitude is steady under different incident angles, while the phase is increased as the incident angle rises from 0° to 50°. To reduce the influence of oblique incidence, we compensate for this phase shift when designing a metasurface reflector.[25] Here, it should be noted that the phase variation is relatively uniform within a frequency range of 14 GHz–16 GHz, and the phase compensation works well in this band. Here, the phase compensation is based on the phase shift at 15 GHz. The initial phase for compensation is set to be phase response under the normal incidence. Accordingly, the operating frequency is selected to be in the range of 14 GHz–16 GHz.

## 3. Configurations and simulations

To verify the performance of proposed shared aperture antenna, a reflector model consisting of 30×30 unit cells with a size of 204 mm×204 mm is designed. In order to reduce the interference of each spot source and avoid blocking the radiated beams, the two spot sources are separately placed at two

predesigned offset focal points. In this design, the two offset focal points are arranged above the midpoint of two edges of the metasurface reflector with a spacing of 150 mm. The positions of feed antennas are governed by half the power bandwidth of the proposed Vivaldi antennas. In our design, half the power bandwidth is 47°. Through the careful optimization, the opening angle between the positions of the feed antennas and the two edges of the metasurface reflector are both 53°, which is slight larger than that in the case for half the power bandwidth to ensure that most of the radiation energy feeds the antennas illuminated on the reflector.

According to Eq. (1), the needed phase distribution $\varphi(x, y)$ of metasurface reflector is superimposed by spatial parabolic phase gradients and spiral phase gradients. The initial phase is arranged in the center of parabolic phase distribution (two midpoints of the reflector edges mentioned in the manuscript). On the other hand, owing to the fact that the amplitude of the proposed unit cell is stable and close to 1 under different incident angles, the influence of amplitude fluctuation can be ignored in the design process of reflector. In the designing process, the amplitude is regarded as uniform and equal to 1. Here, topological charges of $l = -1$ and $l = -2$ are selected as two examples to design $x$ and $y$ polarizations. Accordingly, the phase distributions for $x$ and $y$ polarizations are depicted in Figs. 4(a) and 4(b), respectively. Theoretically, owing to the compensation for spatial parabolic phase gradients, the reflective vortex beams will propagate along the normal direction rather than oblique direction.[22]

The designing process of metasurface reflector is depicted in Fig. 4(c). According to the calculated phase distributions, the model of the metasurface reflector along the $x$ and $y$ polarizations are respectively assembled by the proposed unit cells with corresponding length of $l_x$ and $l_y$, and then superimposing into the entire metasurface.

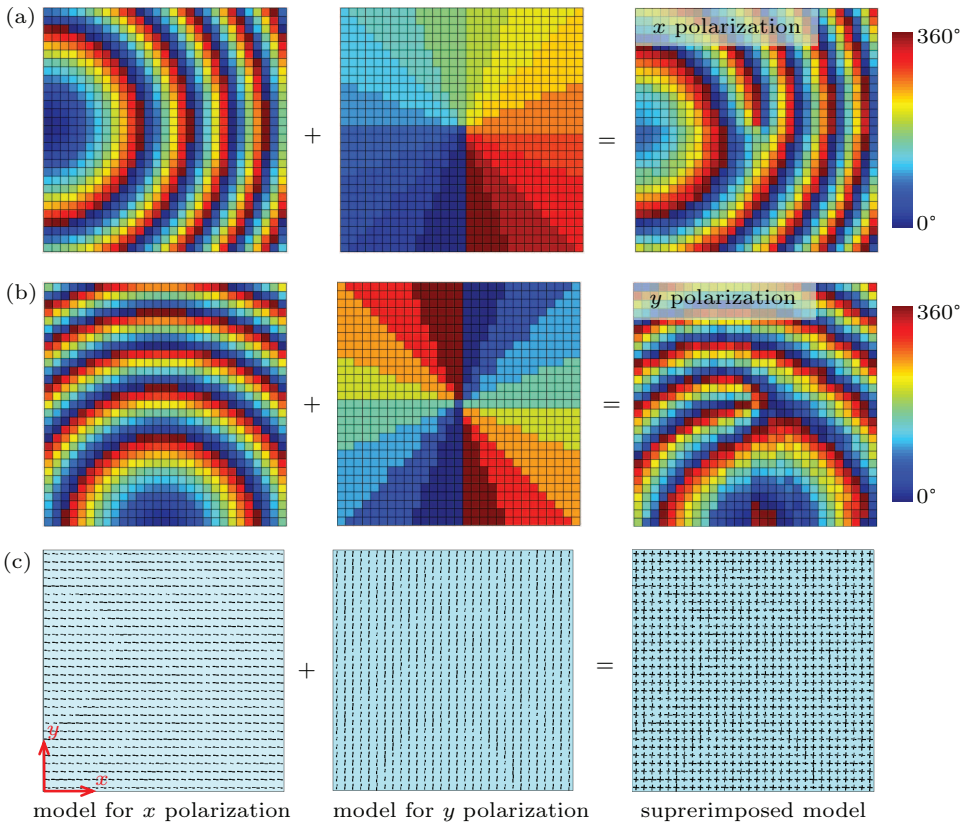



**Fig. 4.** Process of achieving phase distribution of metasurface reflector for (a) $x$ polarization with topological charges $l = -1$, (b) $y$ polarization with topological charges $l = -2$, and (c) model of proposed metasurface reflector.

To provide simple linearly polarized feeds with good radiation directionality, two identical Vivaldi antennas are employed for the metasurface reflector.[26,27] The perspective view of the Vivaldi antenna is shown in the inset of Fig. 5(a).

Firstly, the performances of the proposed Vivaldi antenna are simulated by CST microwave studio. Here, the boundary condition is set to be "open add space". Figure 5(a) depicts the simulated $S_{11}$. It is observed that the $S_{11}$ of the proposed Vivaldi antenna is lower than $-10$ dB in a frequency range from 12 GHz to 18 GHz, which manifests that the Vivaldi antenna matches with impedance within this frequency band. In order to ensure that the angular bandwidth of the radiation beam is fit for the metasurface reflector, the far-field performance of Vivaldi antenna is simulated. Figure 5(b) is the two-dimensional (2D) far-field pattern in $xoz$-plane at 15 GHz. The simulation results indicate that the Vivaldi antenna can radiate the beam (half the power bandwidth of 47° for co-polarized (Co-Pol.) radiation) at a low cross-polarization (Cross-Pol.) level. Ac-

cordingly, it can be inferred from Figs. 5(a) and 5(b) that the proposed Vivaldi antenna is suitable for feed antenna.

By aligning two Vivaldi antennas at the focal points, the proposed shared aperture antenna is obtained. Here, the far-field performances are both simulated. The three-dimensional (3D) far-field results show amplitude null along the propagation direction, which is as expected due to the spiral phase profile. Figures 6(a)–6(c) illustrate the 3D far-field patterns when illuminated by feed antenna I ($x$-polarized waves) at 14 GHz, 15 GHz, and 16 GHz. The realized gains are 17.5 dB, 18.8 dB, and 19.7 dB with the divergence angles of 13°, 12°, and 11°, respectively. Figures 6(d)–6(f) are the results under the incidence of feed antenna II ($y$-polarized waves). The realized gains are obtained as 18.9 dB, 20.8 dB, and 21.9 dB, with the divergence angles of 8°, 8°, and 7°, respectively. The center values (values at the amplitude null) and symmetry characteristics of the vortex beams can be intuitively observed by the far-field patterns. For the $x$-polarized waves, the realized gains of null amplitude at 14 GHz, 15 GHz, and 16 GHz are 10.4 dB, 11.1 dB, and 10.9 dB, respectively. For the $y$-polarized waves, the realized gains of amplitude null at 14 GHz, 15 GHz, and 16 GHz are 0.5 dB, 3.9 dB, and 8.5 dB. It is noticed that the realized gains of amplitude null are much lower than the maximum values of the vortex beam radiations, which manifests the excellent performances of the generated vortex beams. Besides, the radiations of vortex beams are basically symmetrical. The slight deviations can be attributed to the offset positions of feed antennas.

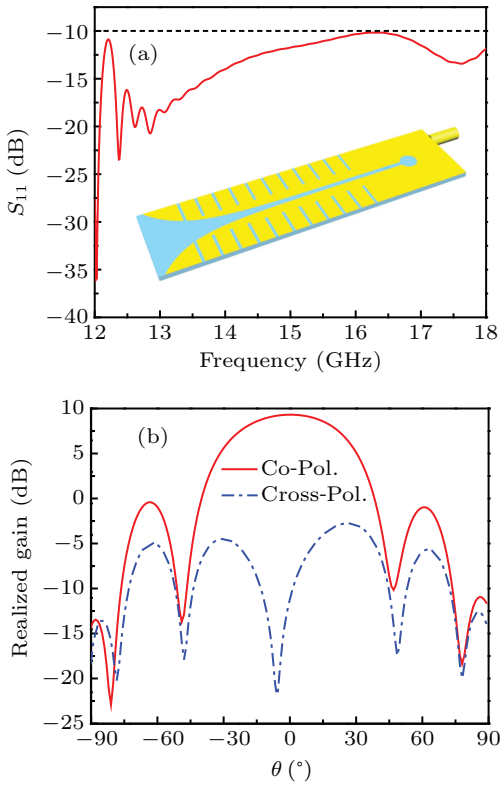



**Fig. 5.** Characteristics of proposed Vivaldi antenna showing (a) $S_{11}$ *versus* frequency, and (b) 2D far-field patterns at 15 GHz.

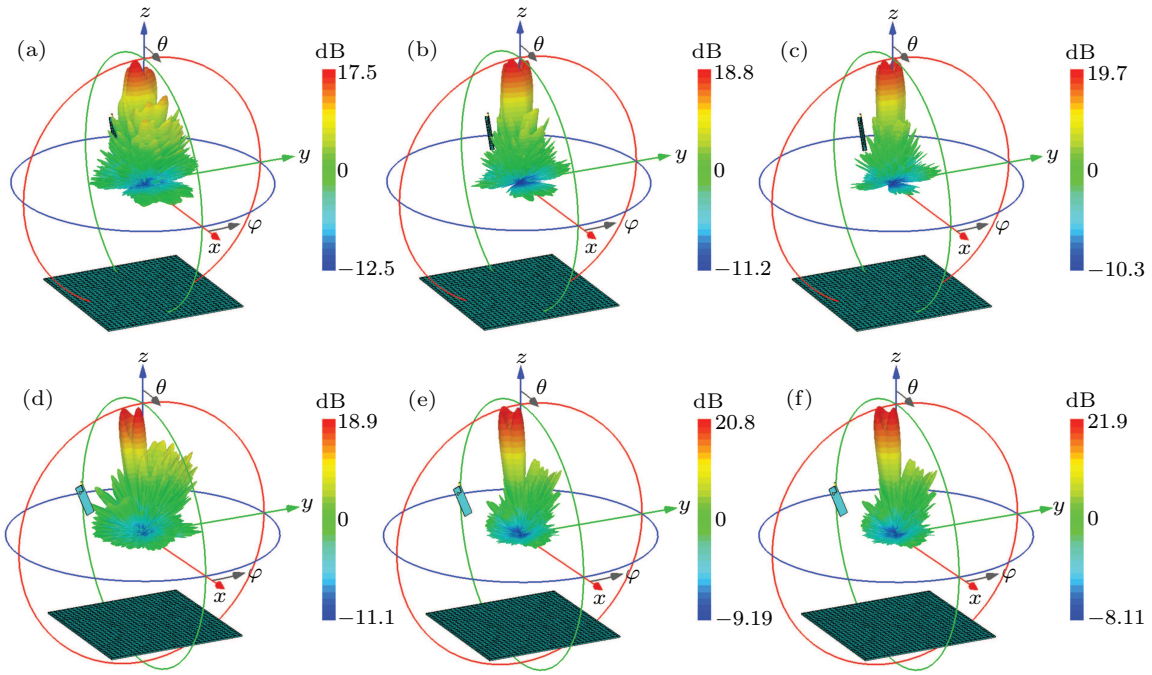



**Fig. 6.** Simulated far-field patterns illuminated by feed antenna I at (a) 14 GHz, (b) 15 GHz, and (c) 16 GHz, and by feed antenna II at (d) 14 GHz, (e) 15 GHz, and (f) 16 GHz.

## 4. Experimental verification

To experimentally validate the feasibility of this design, we first fabricate a prototype of metasurface reflector by low-cost printed circuit board (PCB) technology and then assemble two samples of Vivaldi antenna. The total size of metasurface reflector is 204 mm×204 mm. The prototype is shown in Fig. 7(a) with the inset of unit cells. For the convenience of

experimental operation, the Vivaldi antennas are fixed at the predesigned position by rigid foams. The permittivity of the foams is nearly 1, which is negligible in the measurements. All the experiments are carried out in the microwave anechoic chambers to minimize the reflection from surroundings.

First of all, $S_{11}$ of the proposed shared aperture antenna is measured. Both the simulated and measured $S_{11}$ are presented in Fig. 7(b). It is obvious that the measured $S_{11}$ is lower than $-10$ dB in a frequency range of 14 GHz–16 GHz, which is consistent with the simulation results, indicating that the impedances are matched in the frequency range of 14 GHz–16 GHz. The setup of far-field measurement is depicted in Fig. 7(c). In the measurements, the proposed shared aperture antenna works as a transmitted antenna. The prototype is fixed on a turntable, which can rotate 360° in the horizontal plane. A standard horn antenna is placed 5m away from the prototype serving as a receiving antenna.

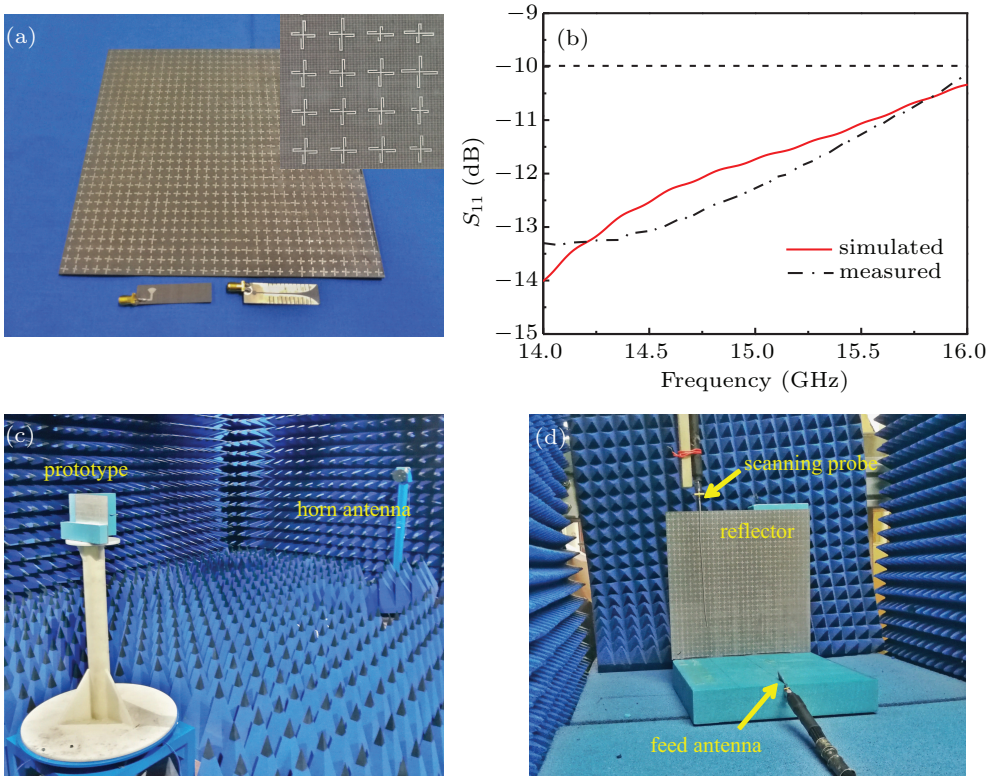



**Fig. 7.** (a) Reflector and feed antennas, (b) $S_{11}$ of the proposed shared aperture antenna, (c) setup for far-field measurement, and (d) setup for near-field measurement.

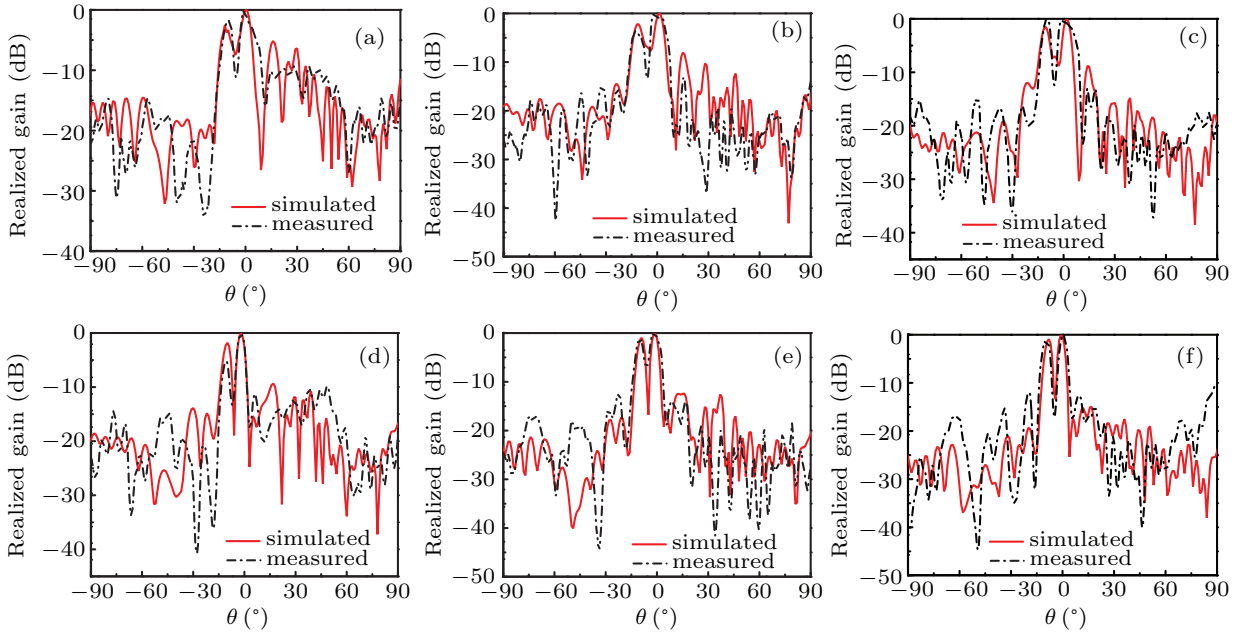



**Fig. 8.** The 2D far-field results in (a) *xoz*-plane at 14 GHz, (b) *xoz*-plane at 15 GHz, (c) *xoz*-plane at 16 GHz, (d) *yoz*-plane at 14 GHz, (e) *yoz*-plane at 15 GHz, (f) *yoz*-plane at 16 GHz.

The 2D far-field results at 14 GHz, 15 GHz, and 16 GHz are illustrated in Fig. 8. Figures 8(a)–8(c) show the results under $x$-polarized incidence ($l = -1$) in $xoz$-plane. Figures 8(d)–8(f) display the results under $y$-polarized incidence ($l = -2$) in the $yoz$-plane. Clearly, the measurement results are in good agreement with simulations. The slight discrepancies between measurement results and simulation results are mainly attributed to the quasi-far-field condition ($2D^2/\lambda$, where $D =$ 204 mm is the diameter of antenna aperture, $\lambda = 20$ mm is the operating wave-length) in the measurement.

Furthermore, to intuitively validate the performance of OAM generation, the simulation results and measurement results of near-field distributions are compared in Fig. 9. The observed plane is parallel to the $xoy$-plane 200-mm away from the metasurface reflector. The near-field scanning technique is used to detect the phase distributions of electric fields. The experimental setup is shown in Fig. 7(d), in which the scanning probe is placed 200-mm away from the metasurface reflector and the scanning plane parallel to the metasurface reflector with a size of 200 mm×200 mm. Here, the scanning step is selected to be 1 mm.

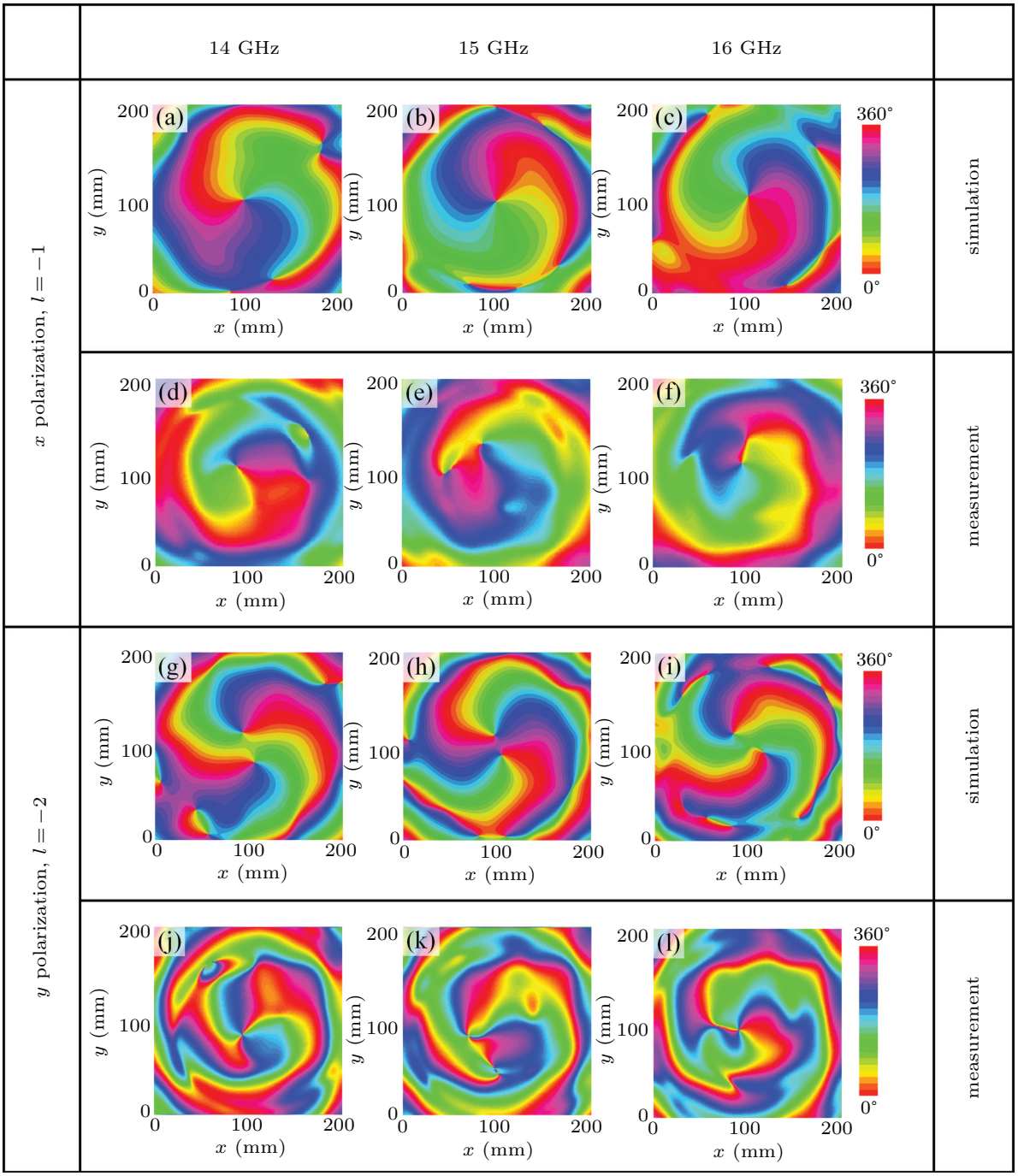



**Fig. 9.** Near-field results of phase distributions: (a)–(c) simulation results of $E_x$-component at 14 GHz, 15 GHz, and 16 GHz; (d)–(f) measurement results of $E_x$-component at 14 GHz, 15 GHz, and 16 GHz; (g)–(i) simulation results of $E_y$-component at 14 GHz, 15 GHz, and 16 GHz; (j)–(l) measurement results of $E_y$-component at 14 GHz, 15 GHz, and 16 GHz.

Figures 9(a)–9(c) and 9(d)–9(f) show the comparisons among the phase distributions of $E_x$-component under the illuminating of feed antenna I ($x$-polarized waves) at 14 GHz, 15 GHz, and 16 GHz. On the other hand, figures 9(g)–9(i) and 9(j)–9(l) display the comparisons among the phase distributions of $E_y$-component under the illuminating of feed antenna II ($y$-polarized waves) at the same frequencies. It is observed that the phase distributions in Figs. 9(a)–9(c) and Figs. 9(d)–9(f) spirally cover 360° in the cutting-plane, while the phase distributions cover 720° in Figs. 7(g)–7(i) and 7(j)–7(l). Accordingly, the good agreement between simulation results and measurement results manifests that the OAM with topological charges $l = -1$ and $l = -2$ is achieved in different polarization states. The differences between measured and simulated near-field distributions can be attributed to the following reasons: the uncertainty in the welding process for feed antenna fabrication, the drift of dielectric parameter, and the misalignment between feed antennas and reflectors. These mentioned errors may be mitigated through optimizing the fabrication and experimental setup in our futureresearch.

In addition, it is noteworthy that the OAM modes generated by the proposed strategy are not limited to $l = -1$ or $l = -2$, but OAM has arbitrary topological charges. According to the mechanism of generating vortex beams, topological charges $l$ can be acquired by rotating the phase distribution $2\pi l$. Here, $l = -1$ and $l = -2$ are just designed as two examples, the OAM with other topological chargers are not designed in this paper for brevity.

## 5. Conclusions

In this work, we propose an effective strategy to design the shared aperture antennas of generating OAM with different topological charges that are dependent on polarization states. As a proof-of-concept, a metasurface reflector antenna that can generate OAM with topological charges $l = -1$ and $l = -2$ is designed and fabricated. The performances of this design are verified numerically and experimentally. Both the simulation results and the experimental results are in good agreement with each other and validate the feasibility of our strategy, indicating good performances of the designed shared aperture antenna. The proposed strategy provides a novel route to designing the shared aperture antenna of generating the vortex beams, which may have applications in the communication systems.

## References


[1] Yu S X, Li L, Shi G M, Zhu C and Shi Y 2016 *Appl. Phys. Lett.* **108** 241901
[2] Karimi E, Schulz S A, Leon I D, Qassim H, Upham J and Boyd R W 2014 *Light-Sci. Appl.* **3** e167
[3] Arikawa T, Morimoto S and Tanaka K 2017 *Opt. Express* **25** 13728
[4] Lloyd S M, Babiker M, Thirunavukkarasu G and Yuan J 2017 *Rev. Mod. Phys.* **89** 035004
[5] Cheng L, Hong W and Hao Z C 2014 *Sci. Rep.* **4** 4814
[6] Uchida M and Tonomura A 2010 *Nature* **464** 737
[7] Niemiec R, Brousseau C, Mahdjoubi K, Emile O and Menard A 2014 *IEEE Antenn. Wirel. Propag.* **13** 1011
[8] Hui X N, Zheng S L, Hu Y P, Xu C, Jin X F, Chi H and Zhang X M 2015 *IEEE Antenn. Wirel. Propag.* **14** 966
[9] Comite D, Valerio G, Albani M, Galli A, Casaletti M and Ettorre M 2017 *IEEE T. Antenn. Propag.* **65** 2123
[10] Lei X Y and Cheng Y J 2017 *IEEE Antenn. Wirel. Propag.* **16** 1357
[11] Li Y, Li X, Chen L W, Pu M B, Jin J J, Hong M H and Luo X G 2016 *Adv. Opt. Mater.* **5** 201600502
[12] Wang H, Li Y F, Chen H Y, Shen Y, Wang J F, Zhang J Q, Zhang A X, Cui T J and Qu S B 2019 *Adv. Opt. Mater.* **7** 1901188
[13] Zhang H F, Kang M, Zhang X Q, Guo W G, Lv C G, Li Y F, Zhang W L and Han J G 2017 *Adv. Mater.* **29** 1604252
[14] Liu H, Mehmood M Q, Huang K, Ke L, Ye H P, Genevet P, Zhang M S, Danner A, Yeo S P, Qiu C W and Teng J H 2014 *Adv. Opt. Mater.* **2** 201400315
[15] Tang S W, Cai T, Liang J G, Xiao Y, Zhang C W, Zhang Q, Hu Z Y and Jiang T 2019 *Opt. Express* **27** 1816
[16] Yu S X, Li L and Kou N 2017 *Opt. Mater. Express* **7** 3312
[17] Veksler D, Maguid E, Shitrit N, Ozeri D, Kleiner V and Hasman E 2015 *ACS Photon.* **2** 661
[18] Guo Y H, Pu M B, Zhao Z Y, Wang Y Q, Jin J J, Gao P, Li X, Ma X L and Luo X G 2016 *ACS Photon.* **3** 2022
[19] Jin D L, Hong J S and Xiong H 2012 *Chin. Phys. Lett.* **29** 104101
[20] Bai W X, Li T L, Gan Q, Cheng R Q and Jiao C Q 2019 *Acta Phys. Sin.* **68** 104101 (in Chinese)
[21] Wei Y Y, Wu Z S, Li H Y, Wu J J and Qu T 2019 *Chin. Phys. B* **28** 074101
[22] Zhang D M, Liao C, Zhou L, Deng X C and Feng J 2018 *Chin. Phys. B* **27** 074102
[23] Zhang L, Wu R Y, Bai G D, Wu H T, Ma Q, Chen X Q and Cui T J 2018 *Adv. Funct. Mater.* **28** 1802205
[24] Xu H X, Cai T, Zhuang Y Q, Peng Q, Wang G M and Liang J G 2017 *IEEE T. Antenn. Propag.* **65** 1797
[25] Wang H, Li Y F, Chen H Y, Han Y, Sui S, Fan Y, Yang Z T, Wang J F, Zhang J Q, Qu S B and Cheng Q 2019 *IEEE Access* **7** 62087
[26] Han Y J, Zhang J Q, Li Y F, Wang J F, Qu S B, Yuan H Y and Yu J B 2016 *IEEE Antenn. Wirel. Propag.* **16** 282
[27] Liu K Y, Guo W L, Wang G M, Li H P and Liu G 2018 *IEEE Access* **6** 63999